The Abdus Salam
International Centre for Theoretical Physics

United Nations
Educational, Scientific and
Cultural Organization

IAEA
International Atomic Energy Agency

2163-28

College on Soil Physics: Soil Physical Properties and Processes under Climate Change

30 August - 10 September, 2010

THE EFFECT OF WIND ON RAINDROP IMPACT AND RAINSPLASH DETACHMENT

Gunay Erpul
University of Ankara
Turkey

The Effect of Wind on Raindrop Impact and Rainsplash Detachment

G. Erpul, L. D. Norton, D. Gabriels

Abstract. *In wind–driven rains, variations in raindrop trajectory and frequency are expected due to the changes in the angle of raindrop incidence. This article presents experimental data on the effects of horizontal wind velocity on rainsplash detachment. In a wind tunnel facility equipped with a rainfall simulator, windless rains and rains driven by horizontal wind velocities of 6, 10, and 14 m s^{-1} were applied to three agricultural soils packed into 20 × 55 cm soil pans with both windward and leeward slopes of 7%, 15%, and 20%. Rain intensity was directly measured with inclined raingauges oriented with respect to the prevailing wind direction. These measurements showed that the actual amount of rainfall intercepted on the soil surface varied widely depending on the angle of rain incidence, which was a function of the rain inclination and slope gradient and aspect. A two–dimensional numerical model was used to estimate wind–driven raindrop trajectories. Rain energy was also measured by a kinetic energy sensor. Theory and measurement showed that an exponential relationship existed between the energy of simulated rainfall and the applied horizontal wind velocity. The experiments led to the conclusion that the wind not only increased the resultant raindrop impact velocity but also altered the angle of raindrop incidence, resulting in variable raindrop impact frequency and impact angle. Accordingly, differential rainsplash detachment occurred depending on the changes in raindrop trajectory and frequency with wind velocity and direction. There were significant differences in the detachment rates between the aspects, and the rates were as much as 44 times greater in the windward slopes than in the leeward slopes.*

Keywords. *Wind–driven rain, Angle of rain incidence, Raindrop trajectory and frequency, Rainsplash detachment.*

Wind–driven rain is described as raindrops falling through a wind field and moving at an oblique direction to the vertical under the effects of both gravitational and drag forces (Choi, 1993). A study of wind–driven rain erosion is thus an attempt to investigate the combined effect of wind and rain on soil erosion processes in situations where wind and rain occur at the same time.

Wind–driven raindrops gain a degree of horizontal velocity, which increases their resultant impact velocity (Umback and Lembke, 1966). Pederson and Hasholt (1995) calculated rain energy with a model using horizontal terminal velocities of raindrops that resulted from the wind velocity under natural rainfall conditions. They suggested an exponential equation for rain energy as a function of rain intensity and wind velocity. Wind–driven raindrops strike the soil surface with an angle deviated from vertical (Van Heerden, 1964; Umback and Lembke, 1966; De Lima, 1989), and this inclination depends on the horizontal velocity component gained from the wind drag. The size distribution and intensity of rain are also altered depending on wind velocity and direction (Struzer, 1972). In fact, angle of rain incidence, which is a function of rain inclination and slope gradient and aspect, determines the rain intensity in wind–driven rains. Sharon (1980) and De Lima (1990) introduced a model to calculate the actual amount of rain intercepted on a sloping surface with respect to the prevailing wind direction.

Rainsplash detachment has been widely accepted as an important process that initiates soil erosion (Ellison, 1947; Young and Wiersma, 1973; Morgan, 1978), and the significance of wind on the process is well documented. Lyles et al. (1969) found that up to 66% more soil detachment occurred at 13.4 m s^{-1} wind velocity than without wind at the same rainfall intensity, duration of exposure, and with clods of the same size. Disrud (1970) observed that more clods were destroyed by wind–driven rain than by windless rain. Additionally, wind shear stress was about half as effective as rain kinetic energy in detaching individual clods (Disrud and Krauss, 1971). Pedersen and Hasholt (1995) measured rainsplash erosion on an event–based scale under natural rainfall and obtained a better correlation between rainsplash detachment and erosivity indexes when wind velocity was taken into account.

Conceptually, most studies of wind–driven rain erosion rely on the effect of horizontal wind velocity to increase the kinetic energy of rain. However, variations in raindrop trajectory and frequency are also expected to accompany the changes in angle of raindrop incidence. Poesen (1985) inserted the cosine of the angle of rain incidence into a rainsplash erosion model to account for variations in kinetic energy dissipation on the different slopes and slope aspects. Sharon (1980) reported that the range in wind–driven raindrop frequency on opposite–facing slopes attained a ratio of 1:2, or even exceeded it in extreme cases for rain inclinations of 40° to 70°. Van Heerden (1964) found that the rainsplash detachment decreased under wind–driven rains,

Article was submitted for review in December 2001; approved for publication by the Soil & Water Division of ASAE in August 2002.

The authors are **Gunay Erpul**, Professor, Department of Soil Science, Faculty of Agriculture, University of Ankara, Turkey, and USDA–ARS National Soil Erosion Research Laboratory, Purdue University, West Lafayette, Indiana; **L. Darrell Norton**, Director, USDA–ARS National Soil Erosion Research Laboratory, Purdue University, West Lafayette, Indiana; and **Donald Gabriels**, Professor, Department of Soil Management and Soil Care, Ghent University, Ghent, Belgium. **Corresponding author:** Dr. L. Darrell Norton, USDA–ARS National Soil Erosion Research Laboratory, 1196 Soil Building, Purdue University, West Lafayette, IN 47907–1196; phone: 765–494–8673; fax: 765–494–5948; e–mail: norton@purdue.edu.

although the detached particles traveled longer distances since wind acted as a transporting agent. The reason why the presence of wind decreased the mass of splashed particles was unknown to the author. This article presents experimental results obtained on the effect of horizontal wind velocity on raindrop impact and rainsplash detachment. The objective is to provide improved insight into the detachment process under wind–driven raindrops.

Materials and Methods

The study was conducted in a wind tunnel rainfall simulator facility at Ghent University in Belgium (Gabriels et al., 1997). The wind tunnel is a closed–circuit, low–speed wind tunnel made of sheet metal. Airflow is generated by an axial fan, 1.5 m in diameter, with 16 adjustable blades driven by a 200 h.p. electric motor. Adjusting the pitch angle of the blades by means of a compressor controls the wind speed, and the minimum free stream wind velocity is 6.0 m s^{-1} in the tunnel. The air current is streamlined as it passes a screen and a 2.60 m long cross–shaped splitter. Windstreams additionally pass a honeycomb system before entering into the working area (test section).

All experiments were carried out in the working area, which is 1.20 m wide and 12 m long and with the ceiling adjustable in height from 1.80 m to 3.20 m. The rainfall simulator consisted of a pipeline with spray nozzles. In this study, we used a continuous spraying system of ten downward–oriented nozzles installed 2 m high and at 1 m intervals over a length of 12 m. Nozzle pressure was kept at 1.50 bars.

Three loess–derived agricultural soils were used in this study: Kemmel 1 sandy loam (57.6% sand, 31.1% silt, and 11.3% clay) and Kemmel 2 loam (37.8% sand, 44.5% silt, and 17.7% clay) from the Kemmelbeek watershed (Heuvelland, West Flanders, Belgium) and Nukerke silt loam (32.1% sand, 52.3% silt, and 15.6% clay) from the Maarkebeek watershed (Flemish Ardennes, East Flanders, Belgium). The soil samples were collected from the A_p horizon and air–dried prior to the experiment. Soil was sieved into three aggregate fractions (1.00 to 2.75 mm, 2.75 to 4.80 mm, and 4.80 to 8.00 mm) and recombined to give a mixture with 28%, 32%, and 40%, respectively, of each size fraction. A 5–kg soil sample was then packed loosely into a 55–cm long and 20–cm wide pan after three fractions of aggregates were thoroughly mixed.

Windless rains and the rains driven by horizontal wind velocities of 6, 10, and 14 m s^{-1} were applied to the soil pan placed at both windward and leeward slopes of 7%, 15%, and 20% (4.0°, 8.5°, and 11.3°, respectively). For each soil and slope aspect, there were three replicates; 36 runs (a total of 216 rainfall simulations) were performed.

The raindrop size distributions for windless and wind–driven rains described by Erpul et al. (1998) were used in this study. The simulated rainfall in the wind tunnel consisted of rather small raindrops ranging from 0.2 to 1.8 mm for windless rains and up to 3 mm for wind–driven rains. The nozzles at 1.5 bar operating pressure delivered a median raindrop size (d_{50}) of 1.00, 1.63, 1.53, and 1.55 mm for windless rain and the rains driven by 6, 10, and 14 m s^{-1} winds, respectively. The d_{25}, d_{50}, and d_{75} values of wind–driven rainfalls were greater than those of windless rainfalls. This is attributed either to the raindrop collisions expected as a result of the greater number of small raindrops per unit volume of air or to the possibility that small raindrops drift farther than large drops from the test section of wind tunnel. There is no significant difference in d_{50} of wind–driven rains, which have smaller "spreading" (d_{25}/d_{75}) and "sorting" ($[d_{75} - d_{25}]/d_{50}$) coefficients compared to the windless rain. In general, the raindrop sizes of wind–driven rainfalls have a narrow range around d_{50}, and the most dominant raindrop size is 1.8 mm.

Rainfall intensity was directly measured with five small collectors on the inclined plane. That is, the collectors were placed next to the soil pan with the same slope and aspect as the soil pan during each run. In this way, the intensity measurements were truly representative of each run without any need for correction due to the rain inclination and slope gradient and aspect (Sharon, 1980; De Lima, 1990).

The mean angle of rainfall incidence between the wind vector and the plane of the surface was calculated from the direct intensity measurement. In fact, wind–driven rain intensity is determined as a function of the angle of rain incidence, which is measured from the normal to the plane of incidence (fig. 1) and given by the cosine law of spherical trigonometry (Sellers, 1965, pp. 33–35):

$$\cos(\alpha \pm \theta) = \cos\alpha\cos\theta \pm \sin\alpha\sin\theta\cos(z_\alpha \pm z_\theta) \quad (1)$$

where

α = raindrop inclination from vertical
θ = slope gradient
z_α and z_θ = azimuth from which rain is falling and azimuth towards which the plane of surface is inclined, respectively.

In order to include the effect of the angle of incidence on the rainfall intensity, the impact efficiency of wind–driven raindrop (ϕ) can be defined by:

$$\phi = \frac{I_a}{I} = \cos(\alpha \pm \theta) \quad (2)$$

where I is the rainfall intensity with respect to a plane normal to the rain vector, and I_a is the actual intensity. Equation 2 indicates that the actual rate of wind–driven raindrop impact per unit area varies with the rain inclination induced by the horizontal wind velocity and the slope gradient and aspect.

We used a two–dimensional analytical model to estimate raindrop trajectories, considering the forces that act on a raindrop in both along–wind and vertical directions. The equations for vertical (z) and horizontal along–wind (x) are as follows (Haasz and Raimondo, 1980; Choi, 1993; Petersen and Hasholt, 1995; Hangan, 1999; De Lima et al., 2002):

$$m\frac{\partial^2 z}{\partial t^2} = mg - \rho_a g \forall - \frac{1}{2} C_d \rho_a \left(\frac{\partial z}{\partial t}\right)^2 A \quad (3)$$

$$m\frac{\partial^2 x}{\partial t^2} = -\frac{1}{2} C_d \rho_a \left(\frac{\partial x}{\partial t}\right)^2 A \quad (4)$$

If raindrops are considered spheres of diameter d (m) and density ρ_w (kg m^{-3}), then the mass of the raindrop is $m = \rho_w/6)\pi d^3$ (kg) with a projected frontal area of $A = \pi d^3/4$ (m^2), and the raindrop volume is $\forall = \pi d^3/6$ (m^3); g is the gravitational acceleration (m s^{-2}), ρ_a is the air density (kg m^{-3}), and C_d is the drag coefficient on the raindrop calculated as a function of Reynolds number (Re):

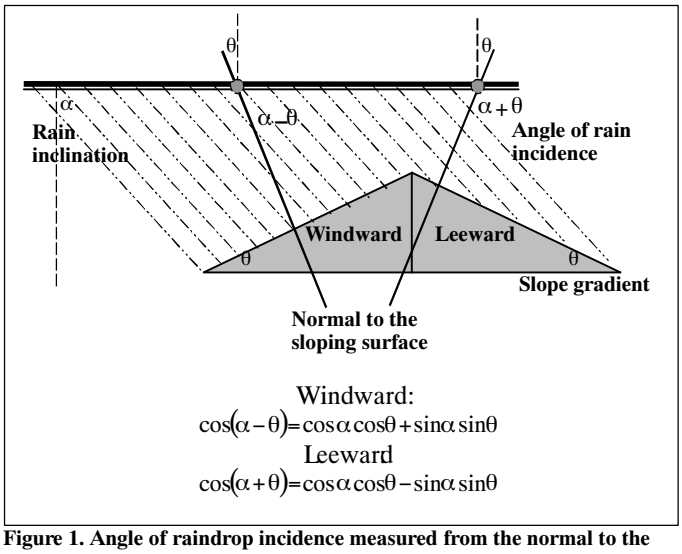

Figure 1. Angle of raindrop incidence measured from the normal to the plane of incidence.

$$\mathrm{Re} = \frac{\rho_a u d}{\mu} \qquad (5)$$

where u is free stream wind velocity (m s^{-1}) and μ is viscosity of air (N s m^{-2}). Drag coefficients were nearly on the constant region of the C_d vs. Re curve (Gunn and Kinzer, 1949) for the calculated Reynolds numbers, which changed from 6.4×10^2 to 1.4×10^3.

Equations 3 and 4 show that the forces acting on the raindrop are due to gravity, buoyancy, and drag. It is here assumed that raindrops reach their terminal velocities in the z–direction and satisfy $m(\partial^2 z/\partial t^2) = 0$, and the x–component of the raindrop velocity is a function of horizontal wind velocity profile, $m(\partial^2 x/\partial t^2) = f(u_{(z)})$. Wind velocity profiles were measured from the soil surface up to the 2–m nozzle height with a vane anemometer and associated recording equipment. The wind velocity profiles above the soil pan were characterized by the following logarithmic equation:

$$u(z) = \left(\frac{u*}{\kappa}\right) \ln\left(\frac{z}{z_o}\right) \qquad \text{for} \quad z > z_o \qquad (6)$$

where

$u(z)$ = wind velocity at height z
z_o = aerodynamic roughness height
$u*$ = wind shear velocity
κ = von Karman's constant.

The boundary layer was set at 0.30 m above the soil pan. Subsequently, the reference shear velocities were derived from the logarithmic wind profiles, assuming a fixed roughness height of 0.0001 m for bare, smoothed soil surface:

$$z = z_o e^{\kappa u/u*} \qquad (7)$$

Calculated reference shear velocities are 0.35, 0.53, and 0.77 m s^{-1} for the reference wind velocities of 6, 10, and 14 m s^{-1}, respectively. Figure 2 represents the mean wind velocity profiles for all measurements at each level, regardless of slope gradient and slope aspect.

It is important here to note that the effect of rain load on the reference wind velocities was unknown during the wind–driven rain simulations because the velocity measurements

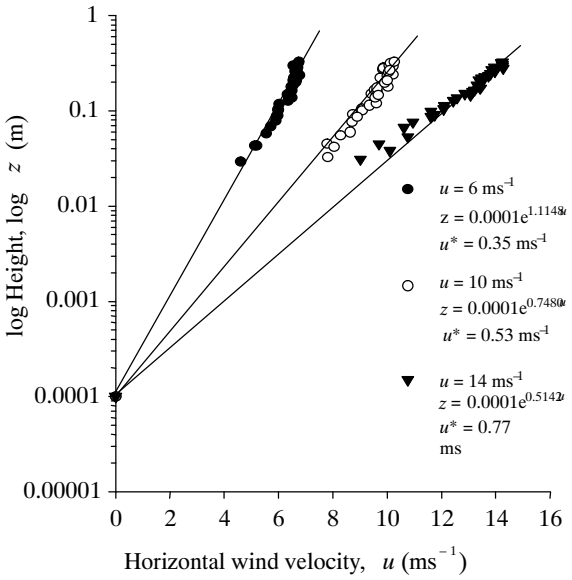

Figure 2. Mean wind velocity profiles for the applied reference wind velocities.

were carried out without rain. We expect that the rain could alter the state of wind, and the velocity could drop to a lower value than the corresponding wind velocity due to the extra drag exerted by wind on the raindrops. Moreover, a water film growth on the soil surface and the soil particle splashes from raindrop impacts certainly generate a surface roughness, thus affecting the boundary layer. Unfortunately, anemometers suitable to work under rainy conditions were not available during the simulations. Therefore, we neglected these effects and used the rainless wind velocity profiles in the analytical solution.

An expression for the horizontal raindrop velocity with respect to the fall height, $(\partial x/\partial t)/\partial z$, was derived using equations 3 and 4 (Pedersen and Hasholt, 1995):

$$\frac{(\partial x/\partial t)}{\partial z} = \frac{3 C_d \rho a}{4 d \rho_w} [(\partial x/\partial t) - u] \qquad (8)$$

The numerical integration of equation 8 was allowed to proceed until raindrops hit the soil surface, and a very small value of relative velocity in the horizontal direction, $[(\partial x/\partial t) - u] = 0.0001$, was used in order to initiate the downward integration.

The energy of simulated rainfalls was also measured by a Sensit kinetic energy sensor (Sensit, 2000). The kinetic energy sensor is a 5–cm ceramic piezoelectric disk. The Sensit works on the piezoelectric effect of a ceramic disk, which produces electric charges proportional to the kinetic energy of impacting raindrops, and essentially has two outputs: kinetic energy units and number of raindrop impacts. The response of the Sensit (voltage output) was calibrated for kinetic energy with vertically falling water drops of known size and known fall velocity. Raindrop size ranged between 2.15 mm and 4.96 mm. The terminal vertical fall velocity of the raindrops was derived from the nomograph of Laws (Laws, 1941). Assuming a spherical raindrop shape, the impact energy of a single raindrop with diameter d is calculated by:

$$KE_{drop} = \frac{\rho_w \forall V^2}{2} \quad (9)$$

where KE_{drop} is the kinetic energy of a single raindrop (J), V is the raindrop impact velocity (m s^{-1}), and the other variables are as defined earlier. The total energy of raindrops is given by:

$$KE = \Xi(KE_{drop}) \quad (10)$$

where Ξ is the number of raindrops and can be calculated from rain intensity and exposure time:

$$\Xi = \frac{ItA}{\forall} \quad (11)$$

where I is the rain intensity (m s^{-1}), and t is the exposure time (s). Equations 9 and 11 together yield:

$$KE = \left(\frac{ItA}{\forall}\right)\left(\frac{\rho_w \forall V^2}{2}\right) = \frac{\rho_w}{2} ItAV^2 \quad (12)$$

A calibration curve for a linear relationship between the raindrop impact energy and the kinetic energy units of the sensor is shown in figure 3.

Soil detachment rates were evaluated by the amount of splashed particles trapped at set distances on a 7–m uniform slope segment. Troughs were placed in both upslope and downslope direction for windless rain, and in upslope and downslope direction, respectively, for windward and leeward slopes for wind–driven rain (fig. 4). For windless rain, splashboards were also positioned to collect side splash.

The soil particles trapped in the collecting troughs were washed, oven–dried, and weighed. Mass distribution curves were then determined for windless and wind–driven rains, of which samples are given in figure 5. Calculation of rainsplash detachment rate was based on the mathematical form of rainsplash erosion (Van Heerden, 1967; Savat and Poesen, 1981; Poesen, 1985):

$$q = \sum_{i=1}^{n} m_i x_i \quad (13)$$

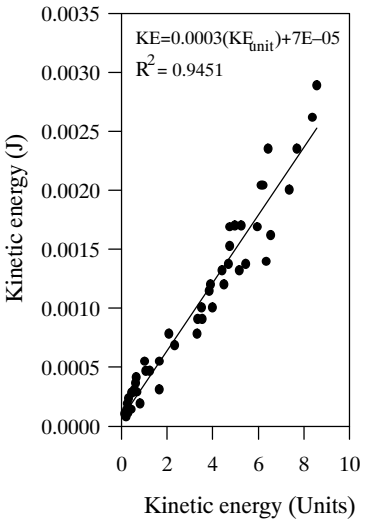

Figure 3. Calibration curve for the Sensit kinetic energy sensor.

where q (gm^{-1} min^{-1}) is the total rainsplash erosion, and m_i (g) is the mass of a particle, which is splashed over a distance x_i (m) measured along the x–axis. Rainsplash detachment rate was estimated from the area under the curves of mass with distance by:

$$D = \frac{1}{At_r} \int \frac{m_i}{x_i} \partial x \quad (14)$$

where

D = rainsplash detachment rate (gm^{-2} min^{-1})

A = surface area of soil pan (0.55 m × 0.20 m = 0.110 m^2)

t_r = time during which rainsplash process occurred (min).

The results were analyzed for two cases of raindrop impact parameters: without angle of incidence and with angle of incidence. Fluxes of kinetic energy and momentum were used as rainfall parameters without angle of incidence:

$$E_r = \Xi_a \left(\frac{1}{2} m V_R^2\right) \quad (15)$$

$$\varphi_r = \Xi_a (m V_R) \quad (16)$$

where

Ξ_a = actual number of raindrops and calculated by $I_a/\forall$ (m^{-2} s^{-1})

E_r = kinetic energy flux (Wm^{-2})

φ_ϱ = momentum flux (Nm^{-2}).

If rainsplash detachment is assumed to be related to the normal component of raindrop impact velocity $[V_R \cos(\alpha \pm \theta)]$ (Heymann, 1967; Springer, 1976; Gilley et al., 1985; Gilley and Finkner, 1985), then fluxes of kinetic energy and momentum, and raindrop impact pressure can, respectively, be calculated by:

$$E_{rn} = \Xi_a \left(\frac{1}{2} m V_R^2\right) \cos^2(\alpha \pm \theta) \quad (17)$$

$$\varphi_{rn} = \Xi_a (m V_R) \cos(\alpha \pm \theta) \quad (18)$$

$$\Gamma = \Xi_a (\rho_w V_R^2) \cos^2(\alpha \pm \theta) \quad (19)$$

where

E_{rn} and φ_{rn} = kinetic energy flux (Wm^{-2}) and momentum flux (Nm^{-2}), respectively, which are related to the normal component of resultant velocity

Γ = total raindrop impact pressure (MPa)

$V_R^2 = V_z^2 + V_x^2$, with $V_z = \partial z/\partial t$ and $V_x = \partial x/\partial t$.

Results and Discussion

Raindrop Impact Frequency

The raindrop fall trajectories influenced by the horizontal velocity and the geometry of the surface, slope gradient and aspect, led to differences in the amount of raindrops hitting the soil surface (eq. 2). In general, as wind velocity and hence rain inclination increased, the amount of rain that was actually intercepted decreased. The effect of slope aspect was also stronger for the higher wind velocities: the angle of incidence attained very high values as the rain inclination and the slope gradient increased on leeward slopes; as a result, the rain intensity reached very low values. For example, the

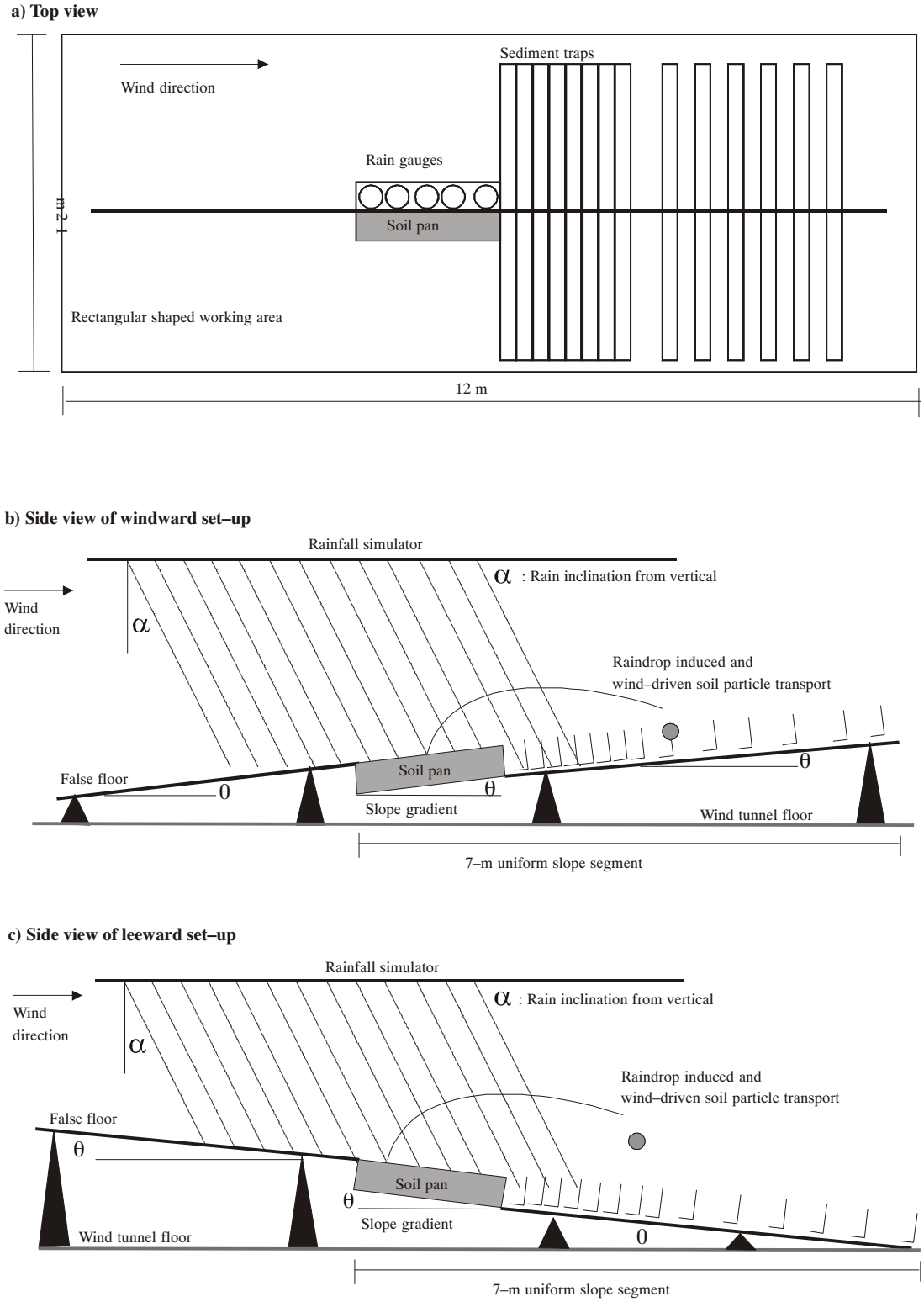

Figure 4. Experimental set–up with soil pan and sediment traps for measurement of rainsplash detachment arranged on the windward and leeward slopes in the wind tunnel.

mean rainfall intensities measured for the rains driven by a 14 m s^{-1} wind incident on the leeward slopes of 8.5° and 11.3° were 42 mm h^{-1} and 34 mm h^{-1}, respectively (table 1).

Few exceptions from equation 2 occurred because the frequency of raindrop impact depended not only on the rain inclination but also on the nozzle number and configuration in the tunnel. There was an increase in the rain intensity for the runs driven by the wind velocities of 10 and 14 m s^{-1} in windward slopes. In those runs, although the rain inclination from vertical was considerably greater compared to the runs driven by the wind velocity of 6 m s^{-1}, the intensity increased since rain from two nozzles reached the test surface. The soil

surface received rain only from one nozzle in the rains driven by the wind velocity of 6 m s^{-1}. However, the effect of the incidence angle on the rain interception was obvious when the test area received the rain from the same number of nozzles. Additionally, in leeward slopes, the placement of the test area was changed to be able to catch an appreciable amount of rain on the test surface as the incidence increases. Because of this, the intensity of windless rains on each slope and the rains driven by the wind velocity of 6 m s^{-1} incident on slopes of 4° and 8.5° were greater than those on the windward slopes.

Notwithstanding these complications, the present results show that the rate of raindrop impact varied widely with wind velocity and direction, leading to different rain fluxes on different facing and sloping surfaces. This observation suggests that different rainsplash detachment rates and different erosion processes can be expected to take place in windward and leeward slopes during a wind–driven rainstorm. For instance, when overland flow generation is retarded due to decreased rainfall interception by a leeward sloping soil surface, wind–driven soil particle transport, or splash drift (Rutin, 1983; De Lima et al., 1992; Gabriels et al., 1998; Goossens et al., 2000), might be the dominant erosion process.

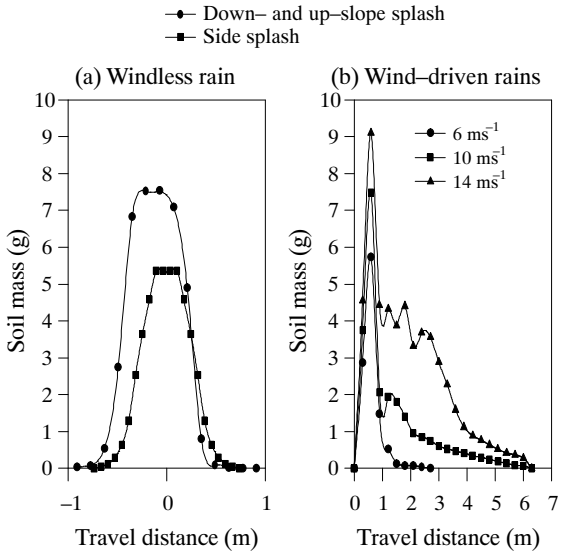

Figure 5. Mass distribution curves used for calculating rainsplash detachment rates. For windless rains (a), negative values stand for downslope and left–side splash, while positive values stand for upslope and right–side splash. For wind–driven rains (b), the particle movement is unidirectional and in the prevailing wind direction (Nukerke silt loam, windward slope of 11.3°).

Table 1. Measured rainfall intensities (I_a) and calculated angle of rain incidence as a function of the rain inclination and slope gradient and aspect for the windless rains and the rains driven by the reference wind velocities of 6, 10, and 14 m s^{-1}.

u (m s^{-1})	$u*$ (m s^{-1})	d_{50} (mm)	α (°)	θ (°)	I_a (mm h^{-1})	α ± θ (°)	ϕ
0 – ww	—	1.00 .97 ≤ d_{50} ≤ 1.04[a]	—	4.0	142	4.0	0.9976
				8.5	140	8.5	0.9890
				11.3	134	11.3	0.9806
6 – ww	0.35	1.63 1.38 ≤ d_{50} ≤ 1.84	53.0 ± 11.5[b]	4.0	90	49.0	0.6561
				8.5	100	44.5	0.7133
				11.3	106	41.7	0.7466
10 – ww	0.53	1.53 1.50 ≤ d_{50} ≤ 1.57	68.2 ± 7.6	4.0	120	64.2	0.4352
				8.5	130	59.7	0.5045
				11.3	131	56.9	0.5461
14 – ww	0.77	1.54 1.51 ≤ d_{50} ≤ 1.57	73.5 ± 6.6	4.0	90	69.5	0.3502
				8.5	103	65.0	0.4226
				11.3	112	62.2	0.4664
0 – lw	—	1.00 0.97 ≤ d_{50} ≤ 1.04	—	4.0	165	4.0	0.9976
				8.5	172	8.5	0.9890
				11.3	179	11.3	0.9806
6 – lw	0.35	1.63 1.38 ≤ d_{50} ≤ 1.84	53.0 ± 11.5	4.0	126	57.0	0.5446
				8.5	112	61.5	0.4772
				11.3	94	64.3	0.4337
10 – lw	0.53	1.53 1.50 ≤ d_{50} ≤ 1.57	68.2 ± 7.6	4.0	92	72.2	0.3057
				8.5	61	76.4	0.2351
				11.3	51	79.5	0.1822
14 – lw	0.77	1.54 1.51 ≤ d_{50} ≤ 1.57	73.5 ± 6.6	4.0	66	77.5	0.2164
				8.5	42	82.0	0.1392
				11.3	34	84.8	0.0906

u = horizontal wind velocity (ww = windward; lw = leeward).
$u*$ = wind shear velocity.
d_{50} = median drop size.
α = rain inclination from vertical.
θ = slope gradient.
ϕ = cosine of angle of rainfall incidence (= cos[α ± θ]).
[a] 95% confidence interval on mean values of d_{50}.
[b] Standard deviation of the average rainfall inclination is given next to the mean value with ± sign.

Angle of Rain Incidence

The rain inclination and angle of rain incidence, which were calculated using equations 1 and 2, are listed in table 1 and shown in figure 6. Calculations indicated that rain inclination increased with wind velocity, and the average values were 53.0° ± 11.5°, 68.2° ± 7.6°, and 73.5° ± 6.6° for the rains driven by 6, 10, and 14 m s^{-1} winds, respectively. The analysis of variance showed that the means were significantly different from each other at the level of $\alpha = 0.05$. Figure 6b reveals that the slope gradient acted differentially on physical raindrop impact: the angle of raindrop incidence gradually decreased in windward slopes and increased in leeward slopes as the slope gradient increased. The incidence angle attained very high values of approximately 70° to 85° in the rains driven by 10 and 14 m s^{-1} winds on the leeward slopes of 4.0°, 8.5°, and 11.3°. In our study with wind–driven raindrops with >50° of inclinations from the vertical, the impact angle appeared to be a significant impact parameter to evaluate the rainsplash detachment along with the impact velocity and frequency. Most experimental evidence indicates that erosion damage varies with the normal component of impact velocity (Ellison, 1947; Heymann, 1967; Springer, 1976).

When raindrops impact a soil surface, the pressure builds up at the raindrop–soil interface. Pressure acting on the contact area leads to a force normal to the soil surface and forces the splash droplets to escape laterally, entraining soil particles. Rainsplash detachment results from these splashes (Huang et al., 1982; Moss and Green, 1983).

Raindrop Impact Energy

Table 2 shows kinetic energies of windless and wind–driven rains measured by the kinetic energy sensor and estimated by the two–dimensional analytical model (eqs. 3 and 4). Figure 7 illustrates the kinetic energy as a function of the horizontal wind velocity for these methods. Two methods led to similar results for windless rains; unfortunately, they provided relatively different results for wind–driven rains. The discrepancy between the methods increased as the wind velocity increased. This was the result of one of the assumptions made for the analytical solution, which is that the reference wind velocity was the *x*–component of the rain velocity vector at the nozzle height. In nature, a raindrop falling vertically gradually gains horizontal velocity until it reaches a state where its horizontal velocity is equal to the wind velocity (Umback and Lembke, 1966). It was not surprising that, in the wind tunnel with very limited fall height and drift length, raindrops falling through the wind profile could not reach a state in which their horizontal velocity was equal to the reference wind velocity.

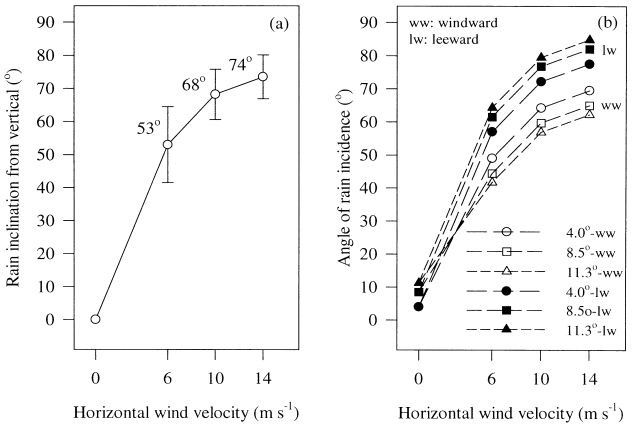

Figure 6. Calculated average rain inclination (a) from vertical and (b) average angle of incidence between the wind vector and the plane of surface as a function of horizontal wind velocity.

Table 2. The kinetic energies (KE) and the resultant impact velocities (V_R) of windless and wind–driven rains measured by the kinetic energy sensor and estimated by the analytical solution.

u (m s^{-1})	d_{50} (mm)	KE (J)	V_R (m s^{-1})	KE = *f*(*u*)[a]	R^2
Kinetic energy sensor					
0	1.00	5.11E–06 (1.25E–06)[b]	4.38 (0.58)		
6	1.63	2.47E–05 (5.99E–06)	4.64 (0.56)	KE = $6E–06e^{0.2184u}$	0.9887
10	1.53	5.51E–05 (8.50E–06)	7.64 (0.60)		
14	1.54	1.07E–04 (1.15E–05)	10.48 (0.57)		
Analytical solution					
0	1.00	1.73E–05	4.10		
6	1.63	6.05E–05	7.31	KE =	0.9902
10	1.53	1.03E–04	10.47	$2E–05e^{0.1712u}$	
14	1.54	1.95E–04	14.13		

u = horizontal wind velocity.
d_{50} = median drop size.
[a] This illustrates a functional relationship that exists between the impact energy and the horizontal wind velocity obtained by the corresponding method in the form of $KE = ae^{bu}$ with *a* and *b* showing the model parameters.
[b] Standard deviation is given in parentheses for the kinetic energy and the resultant impact velocity.

Regardless of differences between the methods, theory and measurement showed that an exponential relationship existed between the rain energy and the horizontal wind velocity (table 2). The increase in rain energy was attributed to the increase in the resultant raindrop impact velocity, since the raindrop size distribution did not change significantly in the rains driven by 6, 10, and 14 m s^{-1} winds in the facility. The following expression was obtained for kinetic energy as a function of wind velocity:

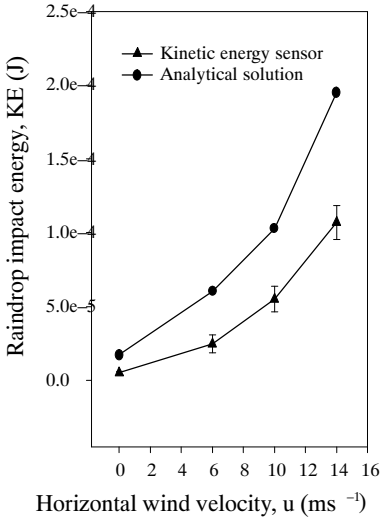

Figure 7. Kinetic energy of simulated rainfall as a function of the horizontal wind velocity evaluated by the kinetic energy sensor and the analytical solution.

$$KE = ae^{bu} \quad (20)$$

where a and b are the parameters of regression. Pedersen and Hasholt (1995) found a similar expression with smaller exponent value (b = 0.12) for natural rainfalls. The effect of wind on large raindrops would not be as great as the effect on small raindrops (Sharon, 1980). Therefore, the exponent values were greater in our equation obtained by the small raindrops in the test facility than that obtained by natural rainfalls. The exponents were approximately 0.17 and 0.22 for the relationship found by the analytical solution and the kinetic energy sensor, respectively (table 2).

The Effect of Wind on Raindrop Impact

Under wind–driven circumstances, rain can consist of deformable raindrops (Haasz and Raimondo, 1980; Hangan, 1999). In addition, there is a possibility of significant changes in raindrop shape, which is a potentially important effect that needs to be considered when estimating rainsplash detachment (Disrud et al., 1969; Riezebos and Epema, 1985; Van Boxel, 1998). However, in our study, practical information was only achieved by examining a simplified model consisting of spherical, non–deformable, independently falling raindrops entering a laminar wind field of known velocity and exposed to gravitational, aerodynamic drag, and inertial forces. Therefore, the effects of wind on raindrop shape, break–up and coalescence, and flow regime were not considered. However, we calculated the effects of wind on velocity, frequency, and angle of raindrop impact to evaluate the rainsplash detachment under wind–driven rain.

Analysis of Pearson correlation coefficients (SAS, 1995, pp. 280–295) summarizes the relationships between the horizontal wind velocity and the examined impact parameters (table 3). The values of V_R and δ are highly correlated with u, and values were greater than 90% for all cases. The value of I_a had a relatively lesser correlation with u in windward slopes. The reason for this was that, as explained previously, I_a depended on the nozzle number and configuration with respect to the source area, as well as the wind velocity. On the other hand, on leeward slopes, to which relatively greater angle of rain incidences corresponded, I_a was to a great extent controlled by the wind velocity (96%). Overall, the results of the correlation analysis showed that the influence of each parameter on the rainsplash process might not be clearly distinguished, but rather confounded, since all were closely correlated and all were functions of the wind.

Table 3. Pearson correlation coefficients among the horizontal wind velocity (u), raindrop impact velocity (V_R), actual rainfall intensity (I_a), and impact angle (δ) for the data from the windward and leeward slopes, and for all data regardless of the slope aspect. Numbers in parentheses are significance levels.

	u	V_R	I_a	δ [a]
Windward				
u	1.00 (0.0)	0.92 (0.0001)	–0.56 (0.0572)	–0.96 (0.0001)
V_R		1.00 (0.0)	–0.34 (0.2808)	–0.79 (0.0024)
I_a			1.00 (0.0)	0.63 (0.0271)
δ				1.00 (0.0)
Leeward				
u	1.00 (0.0)	0.92 (0.0001)	–0.96 (0.0001)	–0.94 (0.0001)
V_R		1.00 (0.0)	–0.85 (0.0005)	–0.74 (0.0056)
I_a			1.00 (0.0)	0.95 (0.0001)
δ				1.00 (0.0)
All data				
u	1.00 (0.0)	0.92 (0.0001)	–0.75 (0.0001)	–0.92 (0.0001)
V_R		1.00 (0.0)	–0.63 (0.0010)	–0.74 (0.0001)
I_a			1.00 (0.0)	0.85 (0.0001)
δ				1.00 (0.0)

[a] δ = raindrop impact angle calculated by $\delta = 90° - (\alpha \pm \theta)$.

Rainsplash Detachment Under Wind–Driven Rain

Rainsplash detachment rates estimated from the mass distribution curves by equation 14 are given in table 4 for three soils. In addition, bar graphs of the detachment rate versus the horizontal wind velocity for windward and leeward slopes are presented in figure 8.

The differential detachment rates occurred depending on the change in raindrop trajectory and rain intensity with the wind velocity and direction. For a particular wind velocity, the detachment rate gradually increased in windward slopes due to the greater raindrop impact frequency with greater impact angles as the slope gradient increased. Conversely, there were lesser raindrop impact frequencies with smaller impact angles in leeward slopes as the slope gradient increased, resulting in lesser detachment rates. Finally, differences in detachment rates between aspects increased as the slope gradient and the wind velocity increased. The detachment rate in windward slope was about 44 times greater than that in leeward slope for the rains driven by a 14 m s^{-1} wind incident on a slope of 11.3° for Nukerke silt loam. For the same runs, the rates were 37 and 28 times greater in the windward slopes than in the leeward slopes for Kemmel 1 sandy loam and Kemmel 2 loam, respectively.

All statistical analyses are performed with individual data points, although mean values are given in table 4. Analyses of Pearson correlation coefficients between rainsplash detachment rate and the rainfall parameters for three soils and for all data regardless of soil type are presented in table 5. The outcome showed that E_r and φ_ϱ had low correlation coefficients with the detachment rate. This occurred because they were unable to account for the changes in raindrop trajectory. Even I_a alone led to a much greater correlation coefficient in each case. Very significantly, the introduction of angle of rain incidence into parameters produced improvements in the coefficients, and each of the parameters (E_{rn}, $\varphi_{\varrho v}$, and Γ) could account for more than 82% of the variation in the detachment rates. This suggests that the angle of rain incidence accounted for the differences in raindrop fall trajectory in connection with the rain inclination and slope gradient and aspect.

A significant result of our findings was large differences between rainsplash detachment on windward and leeward slopes. Pedersen and Hasholt (1995) stressed the necessity of studying slope aspect influence on energy levels under wind–driven rain. Our study indicated that there were dramatic differences in the parameter values between slope aspects, and these were in considerable agreement with variations in the rainsplash detachment rates. Of course, our experimental study with >50° of rain inclination corresponds to the extreme cases of wind–driven rain. In addition, the results were further restricted by the raindrop size distributions that existed in the facility. However, Sharon (1980) reported that in mid–latitudes rain mostly falls at a considerable inclination from vertical, and typical angles of 40° to 70° have been found in rains driven by a wind velocity of 10 m s^{-1}. In such cases, it is likely that slope aspect makes a significant difference in sediment delivery rates to either the

shallow flow–driven or wind–driven transport processes, which are mainly differentiated in terms of overland flow generation (Moss and Green, 1983; Moss, 1988).

Statistical analyses for the rainsplash detachment rate as a power function of E_{rn}, φ_{ov}, and Γ are presented in table 6 for three soils. Units of variables are as presented in table 4. Three models produced different exponent values to which the rainfall parameters were raised and different R^2 values. In every case, the detachment equation with Γ provided the best fit to the data, and R^2 values were >90% (fig. 9). In fact, this was because Γ better accounted for differences in detachment rates between windless and wind–driven rains than E_{rn} and φ_{ov}. The only difference in the calculation of Γ from E_{rn} was the fact that Γ was independent of the raindrop size (eqs. 17 and 19). In our experimental study with rather small raindrops ranging 0.2 to 1.8 mm for windless rains and up to 3 mm for wind–driven rains, the frequency of raindrop impacts appeared more significant in detaching soil than the size of the impacting raindrops. At comparable intensities of windless and wind–driven rains, there were always more impacts in windless rains due to their smaller raindrop size range.

Table 4. Summary of the data for rainfall parameters and measured detachment rates for three soils.

		Rainfall Parameter						Soil Detachment Rate, D (g m^{-2} min^{-1})						
u	θ	I_a	E_r[a]	E_{rn}	φ_r	φ_{rn}	Γ	Nukerke		Kemmel 1		Kemmel 2		
(m s^{-1})	(°)	(mm h^{-1})	(W m^{-2})	(W m^{-2})	(N m^{-2})	(N m^{-2})	(MPa)	Mean	SD	Mean	SD	Mean	SD	n
0 ww	4	142	0.378	0.377	0.173	0.172	157.74	69.10	15.61	71.57	6.13	80.84	11.34	3
	8.5	140	0.373	0.365	0.170	0.168	152.85	71.73	5.99	75.68	12.23	112.15	10.50	3
	11.3	134	0.357	0.343	0.163	0.160	143.82	74.07	23.98	103.53	11.65	117.22	11.39	3
6 ww	4	90	0.269	0.116	0.116	0.076	11.21	6.13	0.59	5.59	0.37	3.98	0.86	3
	8.5	100	0.299	0.152	0.129	0.092	14.72	7.63	1.00	8.07	0.89	5.27	0.80	3
	11.3	106	0.317	0.177	0.137	0.102	17.09	11.28	1.52	10.06	0.80	6.72	1.29	3
10 ww	4	120	0.973	0.184	0.255	0.111	21.55	20.10	0.53	13.86	4.11	14.69	3.72	3
	8.5	130	1.054	0.268	0.276	0.139	31.37	19.04	1.90	17.46	0.40	21.02	3.64	3
	11.3	131	1.062	0.317	0.278	0.152	37.04	28.17	1.18	34.79	0.48	22.49	4.82	3
14 ww	4	90	1.373	0.168	0.262	0.092	19.31	25.14	5.04	11.96	1.93	11.98	2.35	3
	8.5	103	1.571	0.281	0.300	0.127	32.18	42.22	4.61	23.41	2.55	27.20	5.83	3
	11.3	112	1.708	0.372	0.326	0.152	42.63	63.49	8.16	36.50	4.17	40.96	5.90	3
0 lw	4	165	0.440	0.438	0.201	0.200	183.29	83.80	16.32	82.31	6.00	99.28	14.09	3
	8.5	172	0.458	0.448	0.209	0.207	187.78	83.82	20.42	101.48	6.24	131.99	26.60	3
	11.3	179	0.477	0.459	0.218	0.214	192.12	107.28	6.38	136.52	7.22	137.30	17.72	3
6 lw	4	126	0.377	0.112	0.162	0.088	10.81	10.61	0.91	3.03	0.38	6.34	0.81	3
	8.5	112	0.335	0.076	0.144	0.069	7.38	3.65	0.16	1.99	0.13	6.16	0.92	3
	11.3	94	0.281	0.053	0.121	0.053	5.11	3.96	0.36	2.54	0.30	3.50	0.33	3
10 lw	4	92	0.746	0.070	0.195	0.060	8.15	8.08	0.77	6.87	0.80	6.52	0.69	3
	8.5	61	0.495	0.027	0.129	0.030	3.20	2.99	0.30	2.08	0.44	3.11	0.11	3
	11.3	51	0.413	0.014	0.108	0.020	1.61	3.26	0.57	1.87	0.19	2.20	0.13	3
14 lw	4	66	1.007	0.047	0.192	0.042	5.41	7.64	0.44	7.56	1.05	8.07	1.04	3
	8.5	42	0.641	0.012	0.122	0.017	1.42	4.35	0.51	1.98	0.29	3.00	0.47	3
	11.3	34	0.519	0.004	0.099	0.009	0.49	1.43	0.13	0.98	0.17	1.44	0.16	3

I_a = actual rainfall intensity.
E_r and φ_r = fluxes of energy and momentum calculated by equations 15 and 16, respectively.
E_{rn} and φ_{rn} = fluxes of energy and momentum, which are related to the normal component of resultant impact velocity, calculated by equations 17 and 18.
Γ = total raindrop impact pressure calculated by equation 19.
n = number of replications.
[a] Calculation of all rainfall impact parameters (E_r, φ_r, E_{rn}, φ_{rn}, and Γ) was based on the raindrop impact velocity computed from the measurement of kinetic energy by the sensor.

Table 5. Pearson correlation coefficients between the detachment rate (D, g m^{-2} min^{-1}) and the rainfall parameters for three soils and for all data regardless of soil type.

	Rainfall Parameter					
Soil	I_a	E_r	E_{rn}	φ_r	φ_{rn}	Γ
Nukerke	0.73 (0.0001)	0.02 (0.8902)	0.87 (0.0001)	0.29 (0.0140)	0.84 (0.0001)	0.92 (0.0001)
Kemmel 1	0.76 (0.0001)	–0.14 (0.2408)	0.83 (0.0001)	0.20 (0.0968)	0.82 (0.0001)	0.95 (0.0001)
Kemmel 2	0.77 (0.0001)	–0.17 (0.1434)	0.83 (0.0001)	0.17 (0.1596)	0.82 (0.0001)	0.97 (0.0001)
All data	0.75 (0.0001)	–0.10 (0.1144)	0.84 (0.0001)	0.21 (0.0020)	0.82 (0.0001)	0.94 (0.0001)

I_a = actual rainfall intensity.
E_r and φ_r = fluxes of energy and momentum calculated by equations 15 and 16, respectively.
E_{rn} and φ_{rn} = fluxes of energy and momentum, which are related to the normal component of resultant impact velocity, calculated by equations 17 and 18.
Γ = total raindrop impact pressure calculated by equation 19.

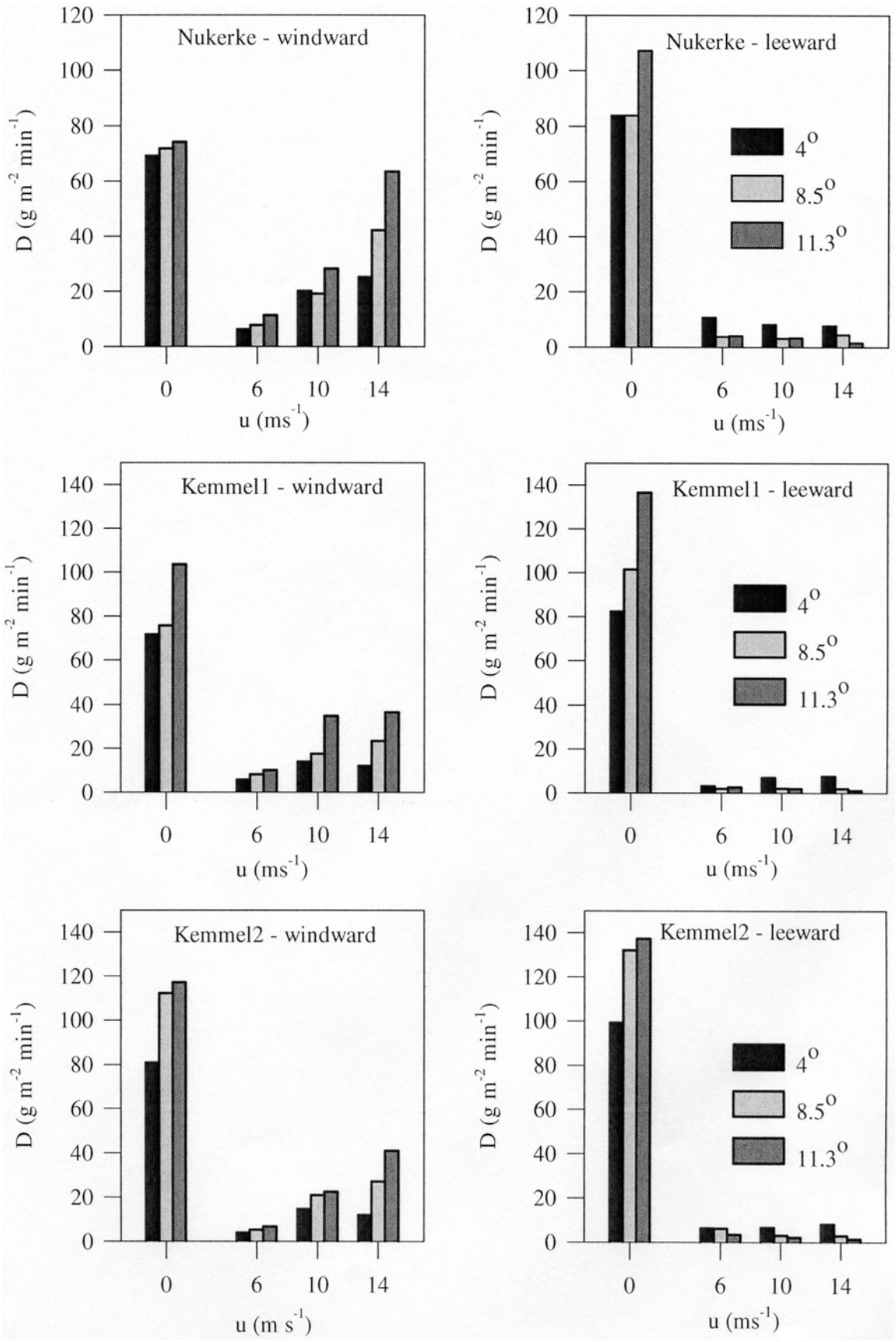

Figure 8. Measured rainsplash detachment rates of Nukerke silt loam, Kemmel 1 sandy loam, and Kemmel 2 loam.

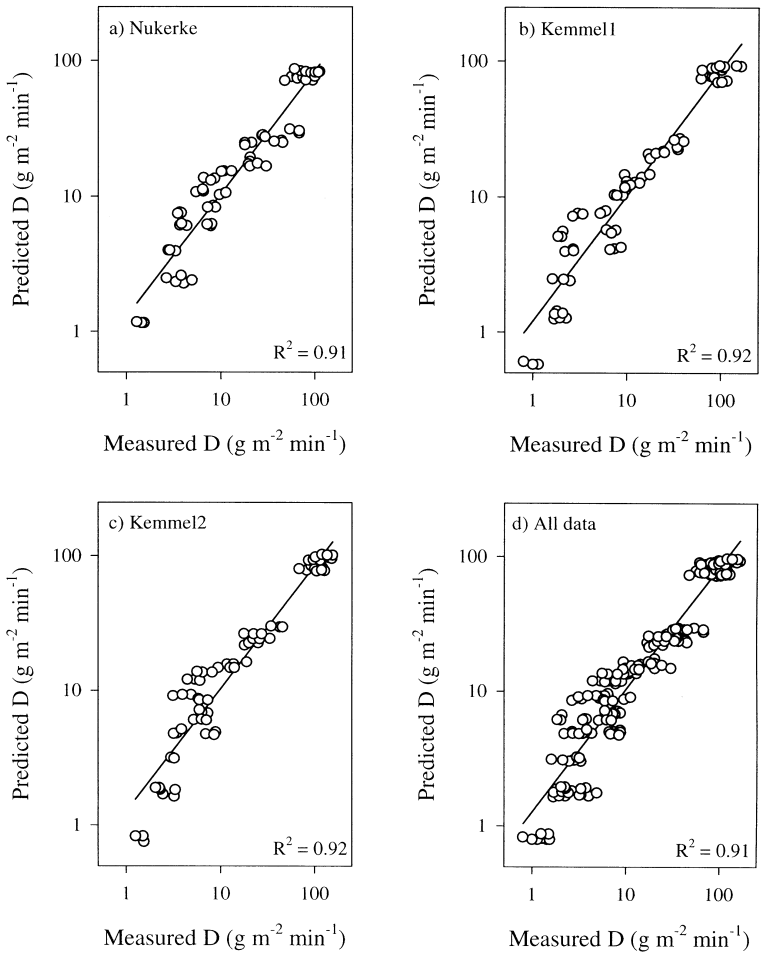

Figure 9. Measured and predicted rainsplash detachment rates of (a) Nukerke silt loam, (b) Kemmel 1 sandy loam, (c) Kemmel 2 loam, and (d) all data irrespective of soil type with the model of $D = K\Gamma^a$.

Table 6. Statistical analyses[a] for the relationship between the soil detachment rate and the selected rainfall parameters.

Soil	$D = KE_{rn}^a$		
	K	*a*	R^2
Nukerke	105.40	0.91	0.79
Kemmel 1	108.64	1.05	0.78
Kemmel 2	109.95	0.98	0.73
All data	108.05	0.98	0.76
	$D = K^{\varphi a}_{rn}$		
	K	*a*	R^2
Nukerke	472.13	1.37	0.77
Kemmel 1	604.40	1.56	0.77
Kemmel 2	595.39	1.51	0.74
All data	554.40	1.49	0.75
	$D = K\Gamma^a$		
	K	*a*	R^2
Nukerke	1.75	0.75	0.91
Kemmel 1	0.94	0.87	0.92
Kemmel 2	1.20	0.84	0.92
All data	1.25	0.82	0.91

[a] Statistical analyses were performed by log–linear regression technique, and the model parameters (K and *a*) in all equations were significant at the P = 0.0001 level for the three soils and all data.

CONCLUSIONS

Only experimental data directly taken on rainsplash detachment has been given in this study, to provide a better insight into the process under wind–driven rains. Results showed that the most widely used parameters, energy and momentum fluxes, to predict soil loss were insensitive to variations in the rainsplash detachment under wind–driven rains. However, introduction of the angle of rain incidence to the parameters significantly improved their ability to predict the mass of sediments detached from the bare soil surface by the impacts of wind–driven raindrops. Our experimental findings, although not tested by the field data, might be a significant step toward development of a model of interrill erosion in which erosion sub–processes of wind–driven rain are well represented.

REFERENCES

Choi, E. C. C. 1993. Simulation of wind–driven rain around a building. *J. Wind Eng. and Industrial Aerodynamics* 46 and 47: 721–729.

De Lima, J. L. M. P. 1989. Raindrop splash anisotropy: Slope, wind, and overland flow velocity effects. *Soil Technol.* 2(1): 71–78.

_____. 1990. The effect of oblique rain on inclined surfaces: A nomograph for the rain–gauge correction factor. *J. Hydrology* 115(1–4): 407–412.
De Lima, J. L. M. P., P. M. Van Dijk, and W. P. Spaan. 1992. Splash–saltation transport under wind–driven rain. *Soil Technology* 5: 151–166.
De Lima, J. L. M. P., P. J. J. F. Torfs, and V. P. Singh. 2002. A mathematical model for evaluating the effect of wind on downward–spraying rainfall simulators. *Catena* 46(4): 221–241.
Disrud, L. A. 1970. Magnitude, probability, and effect on kinetic energy of winds associated with rains in Kansas. *Trans. Kansas Acad. Sci.* 73(2): 237–246.
Disrud, L. A., and R. K. Krauss. 1971. Examining the process of soil detachment from clods exposed to wind–driven simulated rainfall. *Trans. ASAE* 14(1): 90–92.
Disrud, L. A., L. Lyles, and E. L. Skidmore. 1969. How wind affects the size and shape of raindrops. *Agric. Eng*. 50(10): 617.
Ellison, W. D. 1947. Soil erosion studies (7 parts). *Agric. Eng*. 28(5–8): 145–146, 197–201, 245–248, 297–300, 349–351, 407–408, 447–450.
Erpul, G., D. Gabriels, and D. Janssens. 1998. Assessing the drop size distribution of simulated rainfall in a wind tunnel. *Soil and Tillage Research* 45(3–4): 455–463.
Gabriels, D., W. Cornelis, I. Pollet, T. Van Coillie, and M. Quessar. 1997. The I.C.E. wind tunnel for wind and water erosion studies. *Soil Technology* 10(1): 1–8.
Gabriels, D., K. Tack, G. Erpul, W. M. Cornelis, L. D. Norton, and J. Biesemans. 1998. Effect of wind–driven rain on splash detachment and transport of a silt loam soil: A short slope wind tunnel experiment. In *Workshop on Wind and Water Erosion*, 87–93. 17–18 November 1997. Ghent, Belgium: Ghent University.
Gilley, J. E., and S. C. Finkner. 1985. Estimating soil detachment caused by raindrop impact. *Trans. ASAE* 28(1): 140–146.
Gilley, J. E., D. A. Woolhiser, and D. B. McWhorter. 1985. Interrill soil erosion: Part I. Development of model equations. *Trans. ASAE* 28(1): 147–153, 159.
Goossens, D., J. Poesen, J. Gross, and W. Spaan. 2000. Splash drift on light sandy soils: A field experiment. *Agronomie* 20(3): 271–282.
Gunn, R., and G. D. Kinzer. 1949. The terminal velocity of fall for water droplets in stagnant air. *J. Meteorology* 6: 243–248.
Haasz, A. A., and S. Raimondo. 1980. Effectiveness of an air–curtain canopy against precipitation. *J. Wind Eng. and Industrial Aerodynamics* 6: 273–290.
Hangan, H. 1999. Wind–driven rain studies. A C–F D–E approach. *J. Wind Eng. and Industrial Aerodynamics* 81: 323–331.
Heymann, F. J. 1967. A survey of clues to the relation between erosion rate and impact parameters. In *Proc. Conf. on Rain Erosion and Allied Phenomena* 2: 683–760. Farnborough, U.K.: The Royal Aircraft Establishment.
Huang, C., J. M. Bradford, and J. H. Cushman. 1982. A numerical study of raindrop impact phenomena: The rigid case. *Soil Sci. Soc. Amer. J*. 46(1): 14–19.
Laws, J. O. 1941. Measurements of the fall velocity of water drops and raindrops. *Trans. Amer. Geophys. Union* 22: 709–721.
Lyles, L., L. A. Disrud, and N. P. Woodruff. 1969. Effects of soil physical properties, rainfall characteristics, and wind velocity on clod disintegration by simulated rainfall. *Soil Sci. Soc. Am. Proc*. 33(2): 302–306.
Morgan, R. P. C. 1978. Field studies of rainsplash erosion. *Earth Surf. Process.* 3: 295–299.
Moss, A. J. 1988. The effects of flow–velocity variations on rain–driven transportation and the role of rain impact in the movement of solids. *Aust. J. Soil Res*. 26: 443–450.
Moss, A. J., and P. Green. 1983. Movement of solids in air and water by raindrop impact: Effects of drop–size and water–depth variations. *Aust. J. Soil Res*. 21(3): 373–382.
Pedersen, H. S., and B. Hasholt. 1995. Influence of wind speed on rainsplash erosion. *Catena* 24(1): 39–54.
Poesen, J. 1985. An improved splash transport model. *Zeitschrift für Geomorphologie* 29(2): 193–221.
Riezebos, H. T., and G. S. Epema. 1985. Drop shape and erosivity: Part II. Splash detachment, transport, and erosivity indices. *Earth Surf. Process. Landforms* 10: 69–74.
Rutin, J. 1983. Erosional processes on a coastal sand dune, De Blink, Noordwijkerhout. Amsterdam, The Netherlands, University of Amsterdam, Laboratory of Physical Geography and Soil Science.
SAS. 1995. *SAS System for Elementary Statistical Analysis*. Cary, N.C.: SAS Institute, Inc.
Savat, J., and J. Poesen. 1981. Detachment and transportation of loose sediments by raindrop splash: Part I. The calculation of absolute data on detachability and transportability. *Catena* 8(1): 1–18.
Sellers, W. D. 1965. *Physical Climatology*. Chicago, Ill.: University of Chicago Press.
Sensit. 2000. Model V04 Kinetic Energy of Rain Sensor. Portland, N.D.: Sensit Company.
Sharon, D. 1980. The distribution of hydrologically effective rainfall incident on sloping ground. *J. Hydrology* 46: 165–188.
Springer, G. S. 1976. *Erosion by Liquid Impact*. New York, N.Y.: John Wiley and Sons.
Struzer, L. R. 1972. Problem of determining precipitation falling on mountain slopes. *Sov. Hydrol. Selected Papers* 2: 129–142.
Umback, C. R., and W. D. Lembke. 1966. Effects of wind on falling water drops. *Trans. ASAE* 9(6): 805–808.
Van Boxel, J. H. 1998. Numerical model for the fall speed of rain drops in a rainfall simulator. In *Workshop on Wind and Water Erosion*, 77–85. 17–18 November 1997. Ghent, Belgium: Ghent University.
Van Heerden, W. M. 1964. Splash erosion as affected by the angle of incidence of raindrop impact. Unpublished PhD thesis. Lafayette, Ind.: Purdue University.
_____. 1967. An analysis of soil transportation by raindrop splash. *Trans. ASAE* 10(2): 166–169.
Young, R. A., and J. L. Wiersma. 1973. The role of rainfall impact in soil detachment and transport. *Water Resources Res*. 9(6): 1629–1636.